Evaluating Added Benefits of Assimilating GOES Imager Radiance Data in GSI for Coastal QPFs

ZHENGKUN QIN

Center of Data Assimilation for Research and Application, Nanjing University of Information and Science and Technology, Nanjing, China, and Department of Earth, Ocean and Atmospheric Sciences, The Florida State University, Tallahassee, Florida

XIAOLEI ZOU

Department of Earth, Ocean and Atmospheric Sciences, The Florida State University, Tallahassee, Florida

FUZHONG WENG

NOAA/National Environmental Satellite, Data, and Information Service, Washington, D.C.

(Manuscript received 15 March 2012, in final form 28 June 2012)

ABSTRACT

The Geostationary Operational Environmental Satellites (GOES) provide high-resolution, temporally continuous imager radiance data over the West Coast (GOES-West currently known as *GOES-11*) and East Coast (GOES-East currently *GOES-12*) of the United States. Through a real case study, benefits of adding *GOES-11/12* imager radiances to the satellite data streams in NWP systems for improved coastal precipitation forecasts are examined. The Community Radiative Transfer Model (CRTM) is employed for GOES imager radiance simulations in the National Centers for Environmental Prediction (NCEP) gridpoint statistical interpolation (GSI) analysis system. The GOES imager radiances are added to conventional data for coastal quantitative precipitation forecast (QPF) experiments near the northern Gulf of Mexico and the derived precipitation threat score was compared with those from six other satellite instruments. It is found that the GOES imager radiance produced better precipitation forecasts than those from any other satellite instrument. However, when GOES imager radiance and six different types of satellite instruments are all assimilated, the score becomes much lower than the individual combination of GOES and any other instrument. Our analysis shows that an elimination of Advance Microwave Sounding Unit-B (AMSU-B)/Microwave Humidity Sounder (MHS) data over areas where GOES detects clouds significantly improved the forecast scores from AMSU-B/MHS data assimilation.

1. Introduction

It is well known that direct assimilation of satellite infrared and microwave radiances provided by the polar-orbiting meteorological satellites outperforms the assimilation of temperature and moisture retrievals for NWP forecasts (Eyre et al. 1993; Andersson et al. 1994). In 1990s, the Television and Infrared Observation Satellite (TIROS) Operational Vertical Sounder (TOVS) radiance data were directly assimilated at the National Centers for Environmental Prediction (NCEP) and the European Centre of Medium-Range Weather Forecasts (ECMWF; Derber and Wu 1998). In 2005, hyperspectral infrared radiances from the Atmospheric Infrared Sounder (AIRS) in clear-sky conditions were successfully assimilated into operational NWP models (McNally et al. 2006).

Geostationary Operational Environmental Satellites (GOES) provides measurements at infrared channels with high temporal and spatial resolutions, but low spectral resolutions. Assimilation of GOES radiance data in NWP models lagged behind that of polar-orbiting satellite data. In the past, GOES imagery data were used in NWP by assimilating its derived products such as atmospheric motion wind vectors (e.g., cloud-drift winds and water vapor winds) at altitudes assigned based on some auxiliary information from NWP fields (Nieman

Corresponding author address: Xiaolei Zou, Department of Earth, Ocean and Atmospheric Sciences, The Florida State University, 404 Love Building, Tallahassee, FL 32306-4520.
E-mail: xzou@fsu.edu

DOI: 10.1175/MWR-D-12-00079.1

© 2013 American Meteorological Society

et al. 1993; Velden 1996; Velden et al. 1997). The use of auxiliary NWP information and the uncertainty in the height assignment of satellite-derived winds are major obstacles for the assimilation of GOES wind retrievals (Rao et al. 2002). It may also introduce correlations between "observations" (e.g., GOES wind retrieval products) and background fields, which introduces great complications in the estimate of observational error covariances. The impact of GOES wind retrievals on the quality of numerical weather prediction forecasts had thus been not very optimistic as a result of the above-mentioned difficulties (Tomassini et al. 1999; Soden et al. 2001; Goerss et al. 1998; Velden et al. 1998). Further investigations on assimilation of GOES-derived atmospheric motion vectors are needed. Assimilation of cloud-drift winds may be complementary with the clear-sky radiance assimilation.

Efforts have been made to directly and indirectly assimilate observational information from geostationary satellites into NWP systems. Garand and Hallé (1997) assimilated the 6.7-μm outgoing brightness temperature (TB) from *GOES-8* and *-9* through an empirical relationship of this channel with dewpoint depression at upper-tropospheric levels in a global forecast model, found significantly improved with respect to those without satellite data. Köpken et al. (2004) and Szyndel et al. (2005) investigated assimilation of radiances from the Meteosat Visible and Infrared Imager (MVIRI) on board *Meteosat-7* using a global four-dimensional variational data assimilation (4D-Var) system. Stengel et al. (2009) assimilated the Spinning Enhanced Visible and Infrared Imager (SEVIRI) on board *Meteosat-8* using a regional 4D-Var system. GOES imager radiance assimilation not only avoids the need for an arbitrary height assignment, but also directly and realistically simulates satellite-observed radiances given a model atmosphere. While GOES measurements at a specified frequency are the total emitted energy from a volume of the real atmosphere in a specific, frequency-dependent layer of the atmosphere within the instrument's instantaneous field of view (IFOV), model simulations are the total emitted energy from a volume of the model atmosphere in the same layer of the atmosphere within the same instrument's IFOV. GOES radiance assimilation optimally adjusts model state variables so that the simulated radiances fit GOES radiance observations in the maximum likelihood sense (Zou et al. 2001). The development of fast radiative transfer models (McMillin and Fleming 1976; Saunders et al. 1999, 2007; Weng 2007; Han et al. 2007) has allowed for such a direct assimilation of GOES imager radiance to meet the NWP operational forecast requirements.

Although having lower spectral resolution, geostationary satellite instruments provide observations that are extremely valuable for capturing fast-evolving, small-scale mesoscale weather systems that develop within or downstream of a GOES-observing domain (Stengel et al. 2009; Zou et al. 2011). In this paper, we investigate potential impacts of GOES radiance data on coastal quantitative precipitation forecasts (QPFs) near the northern Gulf of Mexico in the presence of other satellite data. Specifically, imager data from *GOES-11* and *GOES-12* is added to the assimilation of the Advance Microwave Sounding Unit-A (AMSU-A), the hyperspectral AIRS, High Resolution Infrared Radiation Sounder (HIRS), GOES Sounder (GSN), the Advance Microwave Sounding Unit-B (AMSU-B) and the Microwave Humidity Sounder (MHS) to assess the complimentary benefit of GOES imager data to these other satellite data for NWP. Since AMSU-B on board the National Oceanic and Atmospheric Administration (NOAA) satellite *NOAA-17* and MHS on board *NOAA-18* and *MetOp-A* have similar channels, MHS will be used hereafter to represent both AMSU-B and MHS for brevity.

The NCEP unified gridpoint statistical interpolation (GSI) analysis code (Wu et al. 2002; Purser et al. 2003a,b) is employed for the study. It is a three-dimensional variational data assimilation (3D-Var) system. The GOES imager data are thinned in both space and time. The assimilation cycle is limited to 12 h to minimize the impact of lateral boundary conditions. A 6-h data assimilation cycling interval is used. This study represents a follow-on study of Zou et al. (2011) who incorporated the *GOES-11/12* thinned imager radiance data into the GSI system and showed the valuable contributions of GOES imager radiances for improved coastal QPFs in the absence of other satellite data.

This paper is organized as follows: The data assimilation experiment setup is provided in the following section. In section 3, the added values of any single type of satellite data (e.g., GOES imager, AMSU-A, AIRS, MHS, HIRS, and GSN) to conventional observations are first compared for improved coastal QPFs near the northern Gulf of Mexico. Numerical experiments assimilating GOES imager radiances together with another type of other satellite observations are then carried out to examine the complimentary benefits of GOES imager data to other data types, and the corresponding results are discussed in section 4. Assimilation of all types of observations and the problems of quality control of some data in the GSI system are analyzed in section 5. Summary and conclusions are provided in section 6.

2. Experiment design

a. The data assimilation system

The NCEP GSI analysis system used in this study is a regional 3D-Var system. A detailed description of the theory and development of the GSI system can be found in Wu et al. (2002). The GSI analysis system is more advantageous than the earlier NCEP spectral statistical interpolation (SSI) analysis system (Derber and Wu 1998) in that it adapts more flexibly to situations where observations are greatly inhomogeneous in terms of their data density and quality. Through an application of recursive filters, the spectral definition of background errors in the SSI analysis system is replaced with a nonhomogeneous gridpoint representation of background errors (Wu et al. 2002; Purser et al. 2003a,b). The GSI system was made available for the NWP community, along with a GSI user's guide (http://www.dtcenter.org/com-GSI/users/index.php) providing a step-by-step procedure for users to install, compile, and run the GSI system on different local computer systems. The GSI has been successfully ported to a Linux platform at The Florida State University (FSU), and results in this study are obtained from the FSU local computing facilities.

b. The satellite data

The GOES and Polar Operational Environmental Satellite (POES) programs provide critical datasets for National Weather Service (NWS) operations. It is composed of two geostationary satellites (e.g., GOES-East and GOES-West) and two polar-orbiting satellites [morning-configured (~1000 local time) and afternoon-configured (~1400 local time) orbits]. These satellites operate in pairs. The geostationary satellites GOES-East and GOES-West cover the East Coast and the West Coast, respectively. The polar-orbiting satellites provide visible, infrared, and microwave data 4 times a day over most of global regions.

The data from GOES imager and sounder, AMSU-A, AIRS, MHS, HIRS, on board GOES/POES measure the total emitted energy in different frequency bands within various instrument's field of view (FOV). Measurements from these instruments are sensitive to atmospheric temperature and water vapor at sounding channels, and to surface emissivity and temperature at window channels. These instrument data can be utilized to improve short-range and medium-range forecast skills (Anderson et al. 2007).

GOES-11 imager has a visible channel 1 with its central wavelength located at 0.65 μm and four infrared channels 2–5, whose central wavelengths are located at 3.9, 6.8, 10.7, and 12.0 μm, respectively. The IFOV diameter at the subsatellite point is 4 km for channels 2, 4, and 5; 8 km for channel 3; and 1 km for channel 1. Channel 4 (10.7 μm) is for surface and cloud-top temperatures. Channels 3 and 5 are mainly used for depicting the upper-level and low-level water vapor, respectively. Channel 2 provides a shortwave infrared radiation for detecting low cloud and fog. The visible channel 1 measures the reflected radiation from the earth and is good for detecting the clouds, aerosols, and surface feature during daytime. This channel is not considered for data assimilation because of its large uncertainty in forward radiative transfer calculations. *GOES-12* imager also has one visible and four infrared channels. Channels 1, 2, and 4 are same as *GOES-11*. However, the central wavelength and spatial resolution of *GOES-12* channel 3 (6.48 μm, 4 km) are slightly different from *GOES-11* channel 3 (6.8 μm, 8 km). *GOES-12* removed channel 5 and added a new CO_2 infrared channel 6 with a central wavelength of 13.3 μm and a spatial resolution of 8 km. The raw data for *GOES-11* and *GOES-12* are resampled and thinned 60- and 40-km resolution, respectively. An advantage to use coarse-resolution radiances is to reduce observation error correlation. A simple bias correction was applied in GOES imager radiance data assimilation by adding a fixed offset of the calculated mean bias using 1-month data from 21 May to 22 June 2008 (Zou et al. 2011).

The AMSU-A is a cross-track scanning microwave radiometer for sounding the atmospheric temperature. It provides a total of 15 channels. There are 12 channels in the frequency range from 50.3- to 57.3-GHz oxygen band for atmospheric temperature profiling from the earth's surface to about 42 km (or 2 hPa). The other three channels are located at 89, 23.8, and 31.4 GHz. The AMSU-A FOV at nadir is about 48 km (Mo 1996). There are a total of 30 FOVs along a single scan line.

The MHS is a cross-track scanning microwave radiometer for sounding the atmospheric water vapor in the troposphere. It measures microwave radiation at the following five channels: 89 (surface), 157, 183.31 $\pm$ 1, 183.31 $\pm$ 3, and 190.31 GHz, respectively (Mo 1999). There are a total of 90 FOVs along each scan line. The nominal spatial resolution of MHS is 15 km at nadir.

AIRS, one of the six instruments carried on board the National Aeronautics and Space Administration's (NASA) *Aqua* satellite, is a hyperspectral infrared sounder providing a total of 2378 thermal infrared radiance observations across a spectrum from 3.7 to 15.4 μm. The spatial resolution for AIRS is 13.5 km at nadir (Aumann et al. 2003).

HIRS/3 is an atmospheric sounding instrument with 1 visible channel (0.6 μm), 7 shortwave infrared channels (3.7–4.6 μm), and 12 longwave infrared channels

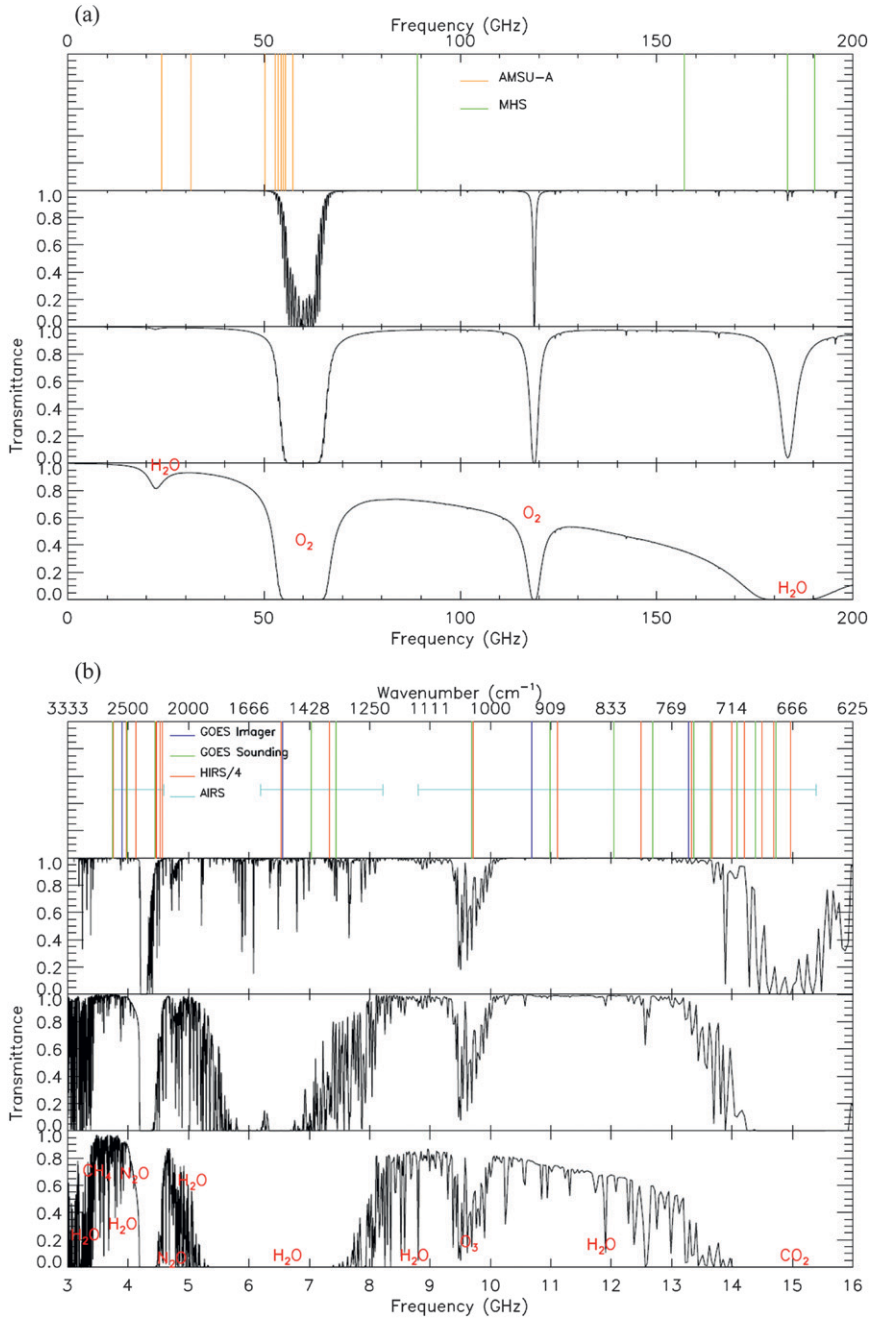

FIG. 1. Transmittance at 100, 500, and 1013 hPa for (a) microwave and (b) infrared channels. Channel frequencies for AMSU-A (orange), MHS (green), GOES imager (blue), GOES sounding (green), HIRS/4 (red), and AIRS (cyan).

(6.7–15 μm). It provides a nominal spatial resolution at nadir of 20.3 km in the visible and shortwave infrared channels and 18.9 km in the longwave infrared band, respectively. The HIRS/4 has the same number of channels as HIRS/3 except for an improvement in observational resolution. The nadir resolution for each channel is approximately 10 km.

The GOES sounder operates independently of the imager and simultaneously samples radiances across large regions of the Western Hemisphere. It contains 18 infrared channels with 7 channels in longwave (12–14.7 μm, channels 1–7), 5 channels in midwave (6.5–11 μm, channels 8–12), and 6 channels in shortwave (3.7–4.6 μm, channels 13–18) bands, and 1 visible channel (0.70 μm).

TABLE 1. List of numerical experiments and satellite data assimilated in each experiment.

Group	Expt name	AMSU-A	AIRS	HIRS/4	HIRS/3	MHS	GSN	GOES imager
First set	$E1_{AMSU\text{-}A}$	✓						
	$E2_{AIRS}$		✓					
	$E3_{HIRS/4}$			✓				
	$E4_{HIRS/3}$				✓			
	$E5_{MHS}$					✓		
	$E6_{GSN}$						✓	
	$E7_{GOES\text{-}Img}$							✓
Single GOES imager channel	$E8_{GOES\text{-}ch2}$							✓ Channel 2 only
	$E9_{GOES\text{-}ch3}$							✓ Channel 3 only
	$E10_{GOES\text{-}ch4}$							✓ Channel 4 only
	$E11_{GOES\text{-}ch5}$							✓ Channel 5 only
	$E12_{GOES\text{-}ch6}$							✓ Channel 6 only
Second set	$GE1_{AMSU\text{-}A}$	✓						✓
	$GE2_{AIRS}$		✓					✓
	$GE3_{HIRS/4}$			✓				✓
	$GE4_{HIRS/3}$				✓			✓
	$GE5_{MHS}$					✓		✓
	$GE6_{GSN}$						✓	✓
Third set	$AE1_{ALL}$	✓	✓	✓	✓	✓	✓	
	$AE2_{ALL\text{-}GSN}$	✓	✓	✓	✓	✓		
	$AE4_{ALL\text{-}MHS\text{-}GSN}$	✓	✓	✓	✓			
	$GAE1_{ALL}$	✓	✓	✓	✓	✓	✓	✓
	$GAE2_{ALL\text{-}GSN}$	✓	✓	✓	✓	✓		✓
	$GAE4_{ALL\text{-}MHS\text{-}GSN}$	✓	✓	✓	✓			✓
Fourth set	$ME5_{MHS}$					✓*		
	$MAE2_{ALL\text{-}GSN}$	✓	✓	✓	✓	✓*		

* Modified QC.

The FOV of the sounder has a nominal resolution of 8 km at nadir, which increases as the viewing angle departs from nadir (Menzel and Purdom 1994).

The regions of the spectrum that are measured by the GOES imager, AMSU-A, MHS, GOES sounding, HIRS/4, and AIRS are compared to an earth (1013 hPa) and two atmospheric (500 and 100 hPa) spectra (Fig. 1). It is seen that in microwave regions, AMSU-A provides measurements at frequencies below 60 GHz in an oxygen absorption band and MHS data are located at higher frequencies above 89 GHz in a water vapor absorption band. The infrared channels from GOES imager, GOES sounding, HIRS/4, and AIRS have a mixed frequency distribution ranging from 3.0 to 16 GHz.

c. *The Community Radiative Transfer Model*

The Community Radiative Transfer Model (CRTM) is a fast radiative transfer model and was developed by the U.S. Joint Center for Satellite Data Assimilation (JCSDA; Weng 2007; Han et al. 2007). It supports a large number of sensors on board historical GOES/POES satellites, new sensors on board Suomi National Polar orbiting-Partnership (NPP), and future sensors from the Geostationary Operational Environmental Satellite-R Series (GOES-R) and the Joint Polar Satellite System (JPSS). It covers the microwave, infrared, and visible frequency regions. Specifically, it is capable of producing model simulations of radiances from all the instruments mentioned in section 2b. The CRTM clear-sky radiance simulation requires vertical profiles of atmospheric temperature and water vapor, surface parameters (e.g., surface temperature and surface wind speed), and satellite geometry parameters as its input. For cloudy radiance simulations, vertical profiles of hydrometeor variables (e.g., cloud liquid water path and ice water path) are also required. The CRTM and its Jacobian module are incorporated into the NCEP GSI data assimilation system, allowing direct assimilations of radiance measurements from all sensors. The CRTM was first released to the public in 2004, and has been substantially improved and expanded since then.

d. *Experiment setup*

A total of 26 data assimilation experiments were carried out for case one, with a 6-h assimilation cycle from 1200 UTC 22 May to 0000 UTC 23 May 2008, followed by a 24-h model forecast (Table 1). The first set consists of a benchmark control experiment assimilating conventional data only ($CTRL_{CONV}$); seven single types of satellite data assimilation experiments by

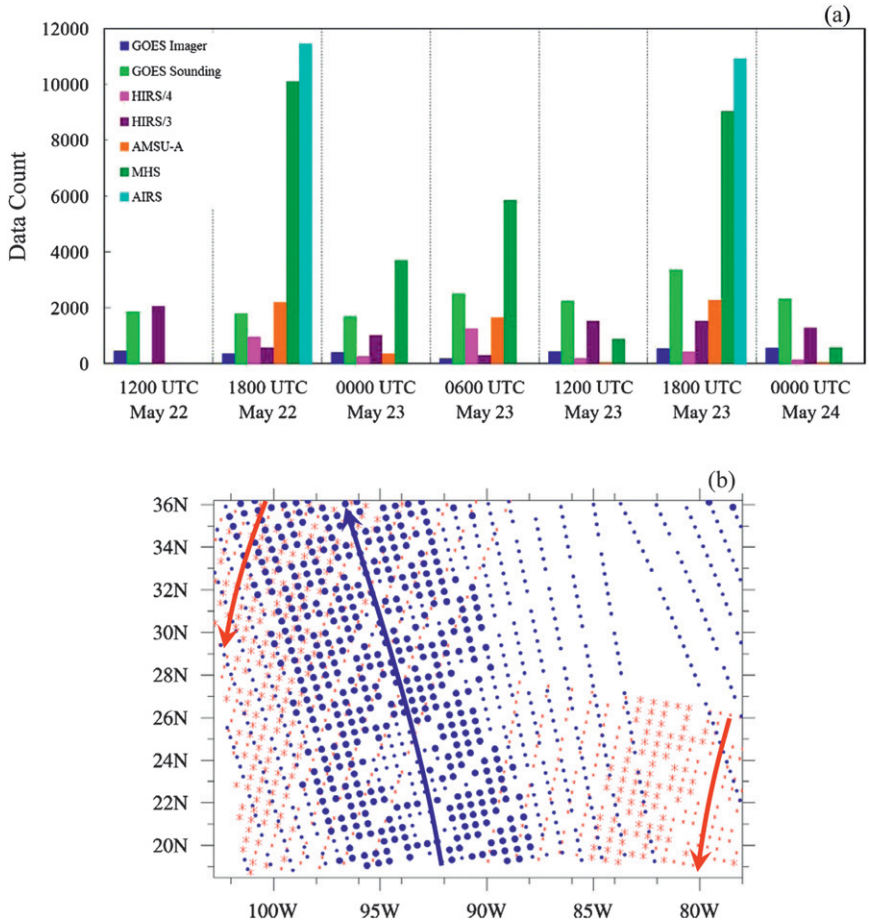

FIG. 2. (a) The total number of assimilated observations from different satellites within three 6-h data assimilation windows centered at 1200 and 1800 UTC 22 May and 0000 UTC 23 May 2008, respectively. (b) Data points of channel 7 from AMSU-A on board *NOAA-18* (dots) and *MetOp-A* (stars) that pass (big dots and big stars) and did not pass (small dots and small stars) QC within 1800 ± 0300 UTC 22 May 2008.

adding AMSU-A ($E1_{AMSU\text{-}A}$), AIRS ($E2_{AIRS}$), HIRS/4 ($E3_{HIRS/4}$), HIRS/3 ($E4_{HIRS/3}$), MHS ($E5_{MHS}$), GSN ($E6_{GSN}$), and GOES imager ($E7_{GOES\text{-}Img}$) data to conventional data; as well as GOES imager single-channel experiments ($E8_{GOES\text{-}ch2}$, $E9_{GOES\text{-}ch3}$, . . . , $E12_{GOES\text{-}ch6}$ for channels 2–6).

The second set of data assimilation experiments consists of six dual types of satellite data assimilation experiments by adding GOES imager radiances to $E1_{AMSU\text{-}A}$, $E2_{AIRS}$, . . . , and $E6_{GSN}$. This set of data assimilation experiments are carried out to evaluate the potential added benefits of GOES imager radiance measurements and will be denoted as AMSU-A ($GE1_{AMSU\text{-}A}$), AIRS ($GE2_{AIRS}$), HIRS/4 ($GE3_{HIRS/4}$), HIRS/3 ($GE4_{HIRS/3}$), MHS ($GE5_{MHS}$), and GSN ($GE6_{GSN}$). The third set of data assimilation experiments consists of three pairs of data assimilation experiments evaluating the impact of GOES imager radiance assimilation in the presence of "all" satellite data: $AE1_{ALL}$ assimilates all satellite data shown in Fig. 2 except GOES imager data, $AE2_{ALL\text{-}GSN}$ is the same as $AE1_{ALL}$ with GSN data eliminated, and $AE3_{ALL\text{-}MHS\text{-}GSN}$ is the same as $AE1_{ALL}$ with both MHS and GSN data eliminated. The $GAE1_{ALL}$, $GAE2_{ALL\text{-}GSN}$, and $GAE3_{ALL\text{-}MHS\text{-}GSN}$ are the same as $AE1_{ALL}$, $AE2_{ALL\text{-}GSN}$, and $AE3_{ALL\text{-}MHS\text{-}GSN}$ except for adding

TABLE 2. The LECT at the ascending node of *NOAA-17* and *-18*, *MetOp-A*, and *Aqua* satellites and the corresponding coordinated universal time (UTC) within the longitudinal zone 82.5°–102.5°W of the main model domain.

Satellite	LECT	UTC	Instruments
NOAA-17	2200	0400–0500	HIRS/3, AMSU-B,
NOAA-18	1345	1945–2045	AMSU-A, HIRS/4, MHS
MetOp-A	0930	1530–1630	AMSU-A, MHS, HIRS/4,
Aqua	1336	1936–2036	AIRS

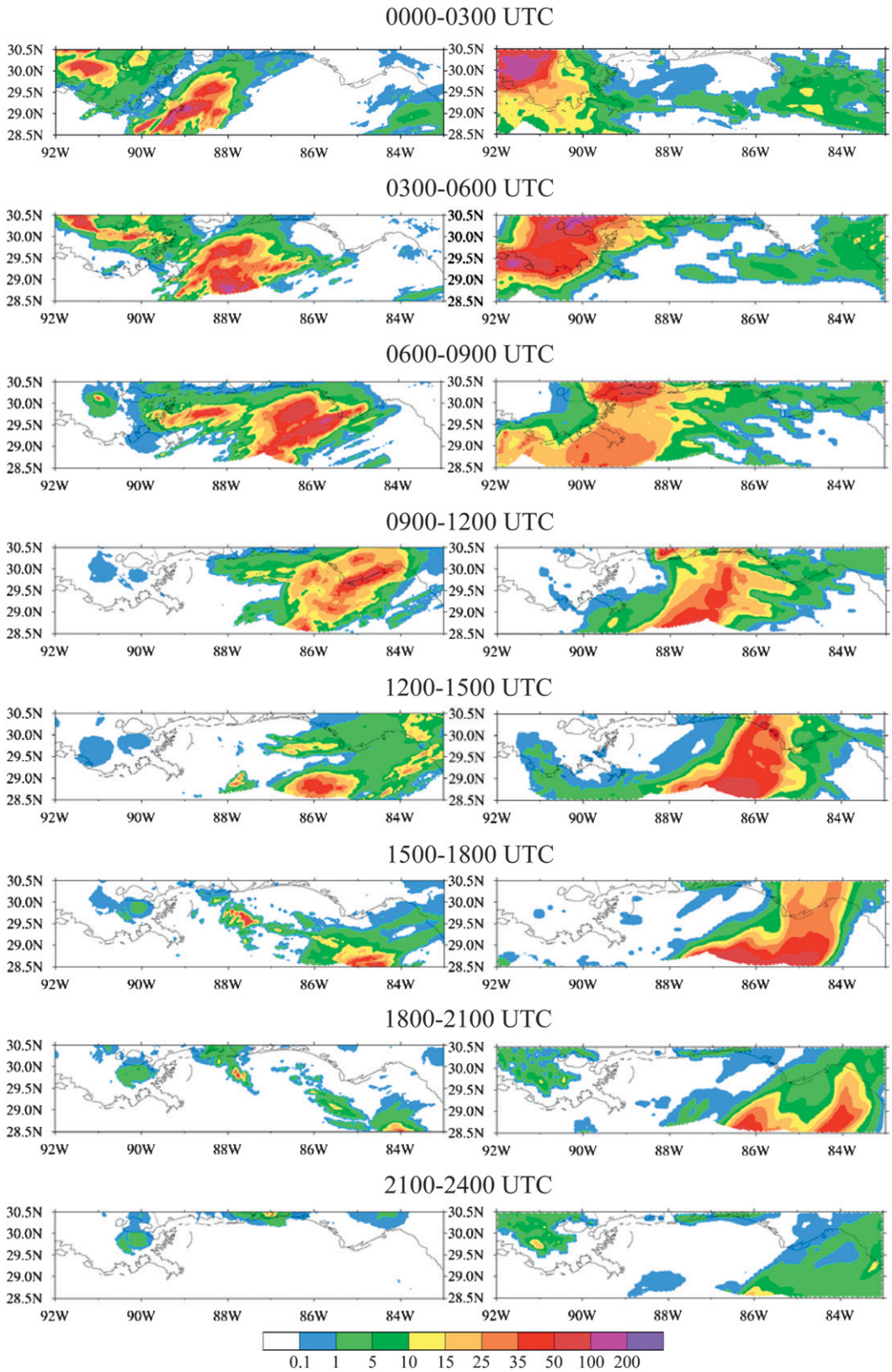

FIG. 3. The 3-h accumulative rainfall (mm) from 0000 to 2400 UTC 23 May 2008 from (left) the NCEP multisensor observations and (right) $E7_{GOES\text{-}Img}$.

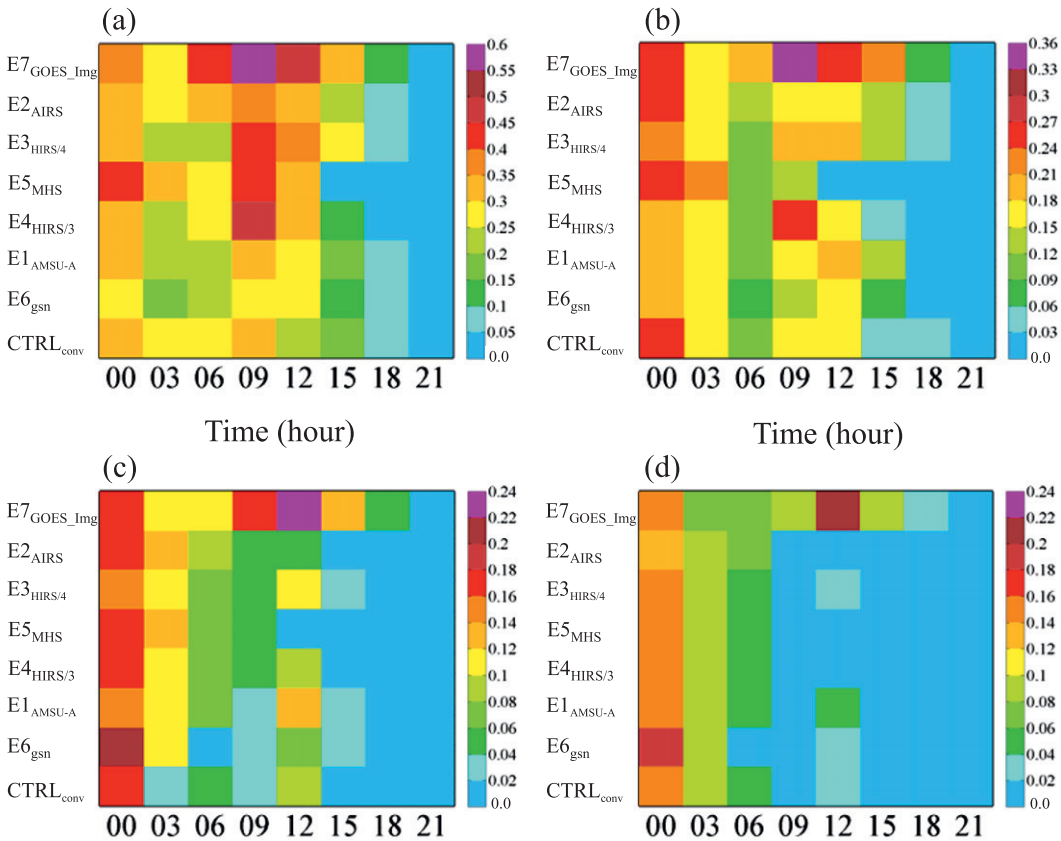

FIG. 4. Threat scores at (a) 1-, (b) 5-, (c) 10-, and (d) 15-mm thresholds for 3-h rainfall forecasts from 0000 to 2400 UTC 23 May 2008 of the experiments $E1_{AMSU\text{-}A}$, $E2_{AIRS}$, $E3_{HIRS/4}$, $E4_{HIRS/3}$, $E5_{MHS}$, $E6_{GSN}$, $E7_{GOES\text{-}Img}$, and $CTRL_{CONV}$.

GOES imager data. The fourth set of data assimilation experiments are designed to show the sensitivity of MHS data assimilation to quality control (QC). Experiments $E5_{MHS}$ and $AE2_{ALL\text{-}GSN}$ are rerun with a modified QC for MHS data and will be denoted as $ME5_{MHS}$ and $MAE2_{ALL\text{-}GSN}$.

Two more cases are included for this last set of experiments. During the 1-month period from 21 May to 22 June 2008, another two coastal precipitation events are found. One occurred from 1800 UTC 20 June to 2100 UTC 21 June 2008 (case 2) and another from 1200 UTC 22 May to 0600 UTC 23 May 2008 (case 3). For case 2, data assimilation is carried out from 0600 to 1200 UTC 20 June 2008, followed by a 27-h model forecast from 1200 UTC 20 June to 2100 UTC 21 June 2008. For case 3, data assimilation is carried out from 0000 to 1200 UTC 22 May 2008, and model forecasts are carried out from 1200 UTC 22 May to 0600 UTC 23 May 2008.

The Advanced Research Weather Research and Forecasting Model (ARW-WRF) is selected as the forecast model The model resolutions and physical parameterization options are the same as described in Zou et al. (2011).

3. Numerical results

a. *Single type of satellite data assimilation*

The case chosen for this study represents a typical weather regime near the Gulf Coast during the late spring and early summer, characterized by a high pressure south of the coast over the water and a low pressure north of the coast over the land. The winds associated with the high pressure system bring warm and moist airs from the Gulf

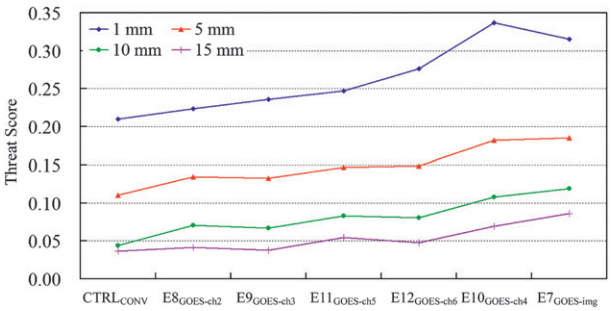

FIG. 5. Threat scores of 3-h accumulative rainfall averaged from 0000 to 2400 UTC 23 May 2008 of model forecast with individual GOES imager channels 2–6 added to conventional observations.

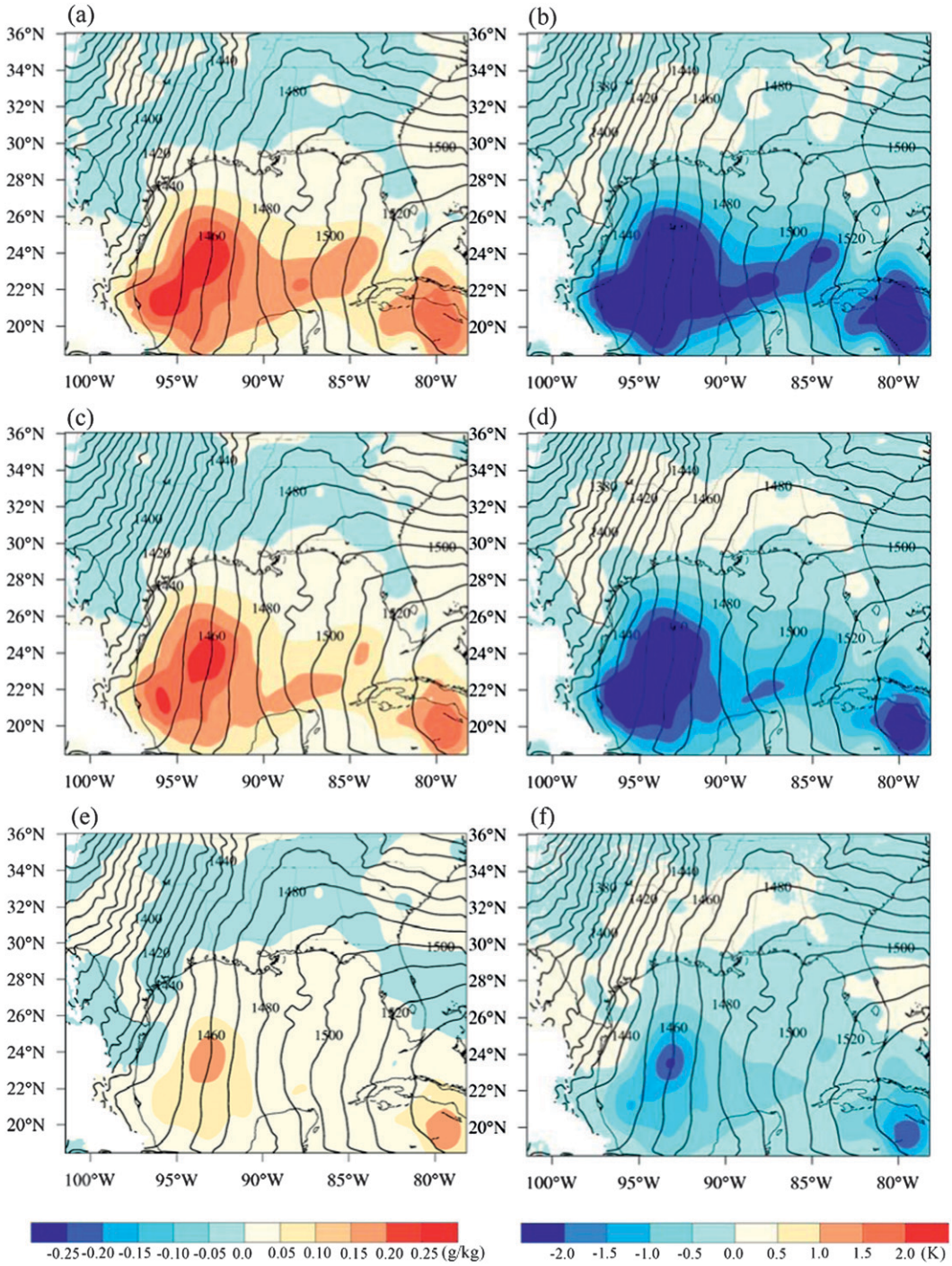

FIG. 6. Analysis differences of (left) 850-hPa mixing ratio (g kg^{-1}) and (right) temperature (K) at 1200 UTC 22 May 2008 (a),(b) between $E7_{GOES\text{-}Img}$ and $CTRL_{CONV}$; (c),(d) between $E10_{GOES\text{-}ch4}$ and $CTRL_{CONV}$; and (e),(f) between $E12_{GOES\text{-}ch6}$ and $CTRL_{CONV}$. The 850-hPa geopotential at 1200 UTC 22 May 2008 from $CTRL_{CONV}$ are shown in contours.

of Mexico to the coastal regions, and the winds associated with the low pressure system bring the cool and dry airs from the north to the coastal regions. When these two air masses met, thunderstorms develop and bring heavy rains to the coastal region of Gulf of Mexico. A synoptic overview can be found in Zou et al. (2011).

We first compare the impacts of satellite radiance assimilation on coastal QPFs near the northern Gulf of

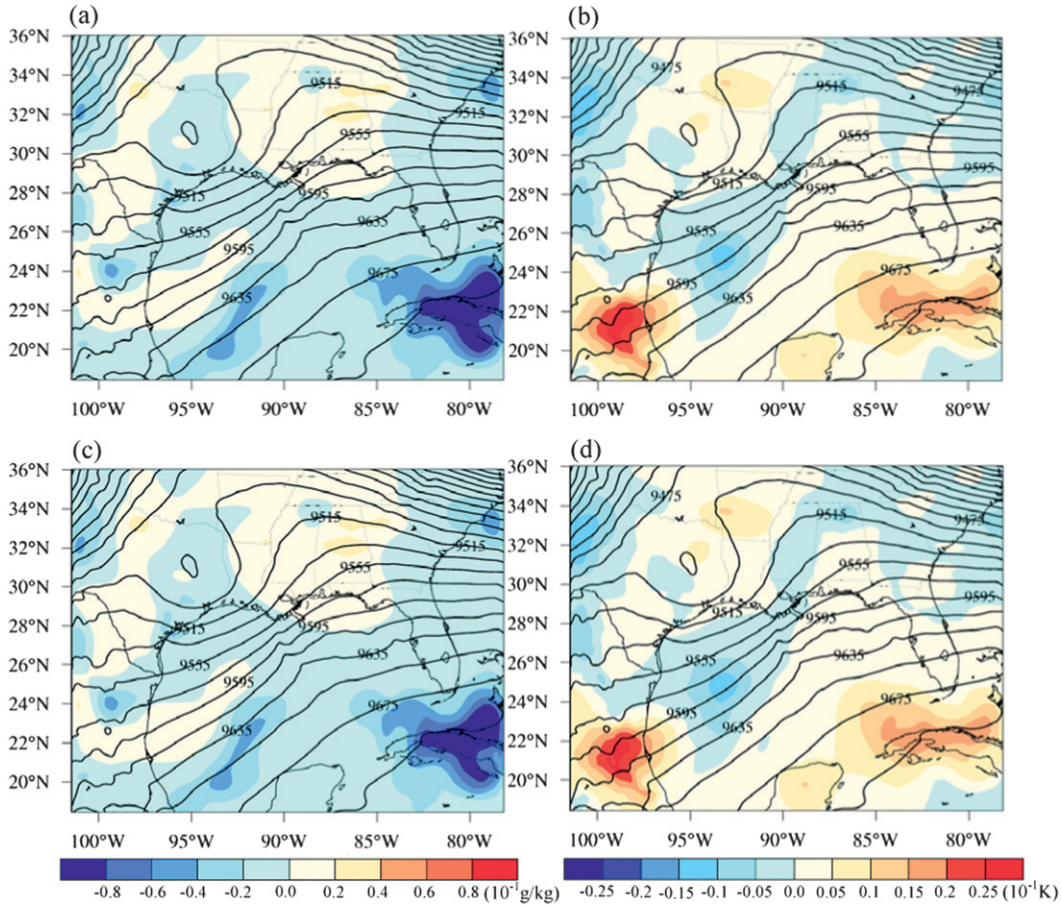

FIG. 7. Analysis differences of (left) 300-hPa mixing ratio (10^{-1} g kg^{-1}) and (right) temperature (10^{-1} K) at 1200 UTC 22 May 2008 (a),(b) between $E7_{GOES\text{-}Img}$ and $CTRL_{CONV}$ and (c),(d) between $E10_{GOES\text{-}ch3}$ and $CTRL_{CONV}$. The 850-hPa geopotential at 1200 UTC 22 May 2008 from $CTRL_{CONV}$ is shown in contours.

Mexico among seven different satellite instruments. The total data counts from various satellite instruments that are assimilated in GSI are provided in Fig. 2a. The data counts from GOES imager and GOES sounder instruments in a fixed model domain are stable in time as expected for geostationary satellites. Data count from a specified satellite peaks in a time zone whose local time is close to the local equator crossing time (LECT) and LECT plus 12 h of this satellite. For example, AMSU data peaks for data assimilation at 0600 and 1800 UTC since the local times of the model domain during 0300–0900 and 1500–2100 UTC time windows are close to the LECT of both *NOAA-18* and *MetOp-A* (Table 2). Data count also depends on orbital gap and where the model domain on the globe. An example of data coverage is provided in Fig. 2b for channel 7 from AMSU-A on board *NOAA-18* and *MetOp-A* within a 6-h time window (i.e., 1800 ± 0300 UTC 22 May 2008). *MetOp-A* is a morning-configured polar-orbiting satellite with its LECT at 0930 local time and *NOAA-18* is an afternoon-configured polar-orbiting satellite with its LECT at 1345 local time. During the 6-h data window for the assimilation experiment conducted at 1800 UTC, observations from *MetOp-A* descending node and *NOAA-18* ascending node are available in the model domain (Fig. 2a). The *MetOp-A* and the *NOAA-18* swaths in Fig. 2a start from 1500 UTC 22 May 2008 from the east.

Figure 3 presents the (Next Generation Weather Radar) NEXRAD-based observations of 3-h accumulative rainfall from 0000 to 2400 UTC 23 May 2008, as well as model-predicted 3-h accumulative rainfall distributions from the experiment $E7_{GOES\text{-}Img}$ over the area within which the threat scores of precipitation are calculated (Anthes et al. 1989). The maximum amount of the observed rainfall moves northeastward from west of the Gulf during the first 6–9 h while intensifying, then southeastward while weakening after 0900 UTC 23 May 2008. Model forecasts from GOES imager

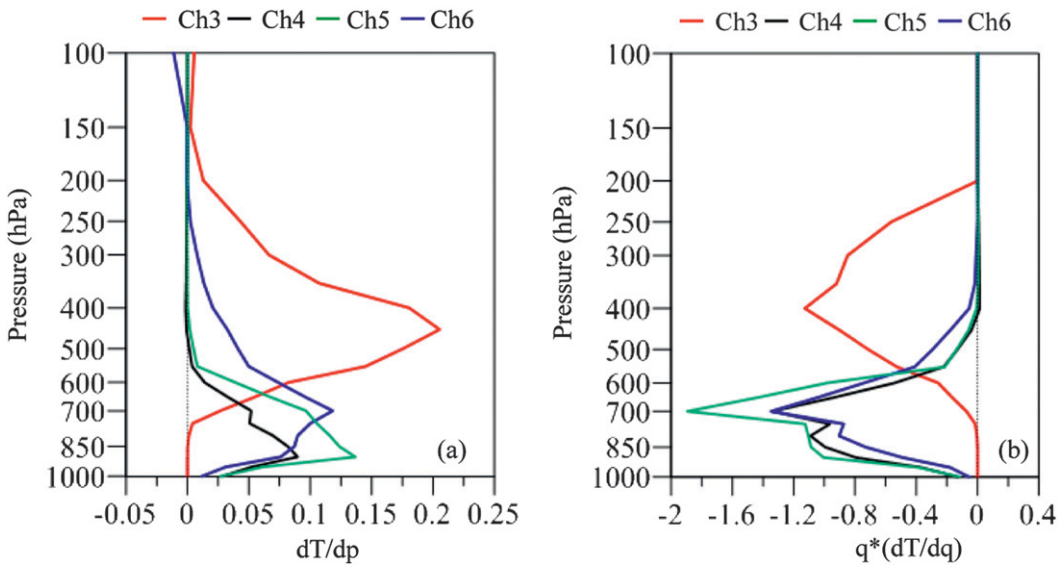

FIG. 8. Mean Jacobian of brightness temperature with respect to (a) temperature and (b) mixing ratio for *GOES-11/12* imager channels 3 (red), 4 (black), 5 (green), and 6 (blue) for real-case profiles that passed GSI quality control at 1200 UTC 22 May 2008 from experiments $E7_{GOES\text{-}Img}$.

radiance assimilation experiment ($E7_{GOES\text{-}Img}$) captures the general features of the movement of this rainfall event except for rainfall amount. The model overpredicts the rainfall amount at the beginning and end of the day. Please note that the NEXRAD observations are confined within a certain distance from radars located over the land and rainfall farther into the ocean is not observed. The threat scores of model-predicted 3-h accumulative rainfall at 1-, 5-, 10-, and 15-mm thresholds during this 24-h time period are shown in Fig. 4. The skill of coastal QPFs decreases with the increases of forecast length. All seven single-type of observation experiments produce positive impacts on QPFs except for $E5_{MHS}$ and $E6_{GSN}$. The GOES imager radiance assimilation experiment $E7_{GOES\text{-}Img}$ outperforms all other experiments including $E1_{AMSU\text{-}A}$, $E2_{AIRS}$, $E3_{HIRS/4}$, $E4_{HIRS/3}$, $E5_{MHS}$, $E6_{GSN}$, and $CTRL_{CONV}$. The rainfall forecasts from the MHS and GOES sounder data assimilation experiments $E5_{MHS}$ compare least favorably with observations.

In $E7_{GOES\text{-}Img}$, radiance measurements from five different channels (channels 2–6) are assimilated. The GOES imager channel 1 is not included in the assimilation because of the large uncertainty in forward radiative transfer calculations. To see which channel is most crucial for the positive impacts on coastal QPFs seen in Fig. 5, a set of GOES imager single-channel experiments ($E8_{GOES\text{-}ch2}$, $E9_{GOES\text{-}ch3}$, . . . , $E12_{GOES\text{-}ch6}$) are carried out. Channel 4 at 10.7 μm makes the largest impact. The CO_2 infrared channel 6, which has a central wavelength of 13.3 μm, is of secondary importance. The low-level water vapor channel 5 is slightly more important than the upper-level water vapor channel 3. The near-infrared radiation channel 2 is least important for improving QPFs near the Gulf Coast of the case studied.

Figure 6 provides the analysis differences of mixing ratio and temperature at 850 hPa and 1200 UTC 22 May 2008 between GOES imager all-channel experiment ($E7_{GOES\text{-}Img}$) and the control experiment $CTRL_{CONV}$, the differences between the experiment assimilated additional GOES imager channel 4 ($E10_{GOES\text{-}ch4}$) and $CTRL_{CONV}$, as well as the differences between the experiment assimilated additional GOES imager channel 6 ($E12_{GOES\text{-}ch6}$) and $CTRL_{CONV}$. The geopotential distribution from $CTRL_{CONV}$ at the same pressure level and same time is also shown in Fig. 6. It is noticed that the mixing ratio and temperature analyses become systematically wetter and colder over the ocean, with the maximum analysis differences located in the western Gulf region where *GOES-11* and *GOES-12* data are most populated [see Figs. 2 and 3 in Zou et al. (2011)]. Such an adjustment in mixing ratio is important and allows moister air be brought from the Gulf of Mexico to the coastal regions. The temperature adjustment discourages the northwestward movement of the subtropical high pressure system, which allows the modeled convection to move southeastward as observed in the subsequent times. Most of the analysis differences between $E7_{GOES\text{-}Img}$ and $CTRL_{CONV}$ (Figs. 6a,d) in the low troposphere come from the assimilation of GOES imager channels 4 ($E10_{GOES\text{-}ch4}$) and 6 ($E12_{GOES\text{-}ch6}$), which is inferred from the results of the single-channel experiments (Figs. 6b,c,e,f). The analysis differences of mixing

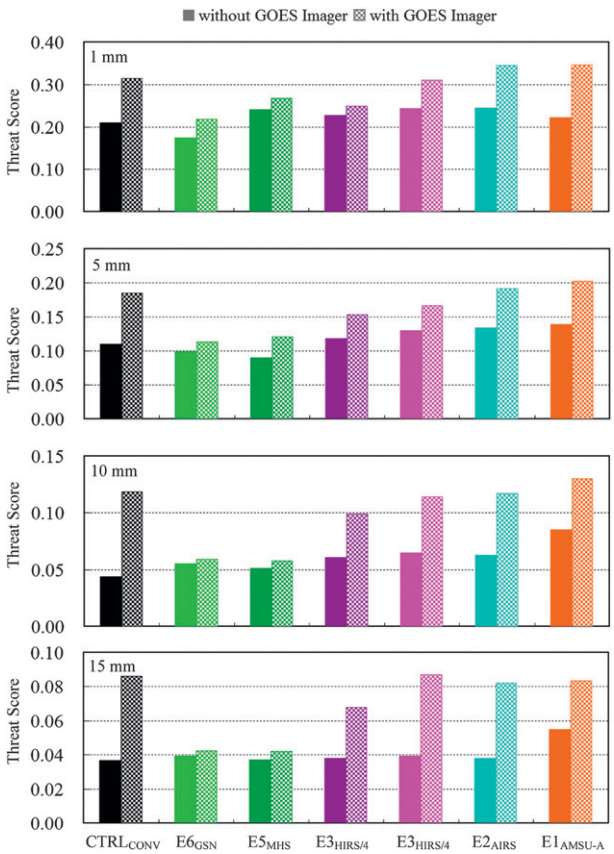

FIG. 9. The average 3-h threat score at 1-, 5-, 10-, and 15-mm thresholds from 0000 to 2400 UTC 23 May 2008 of forecasts without (solid bars) and with (dashed bars) GOES imager data is added to conventional data and different types of satellite data.

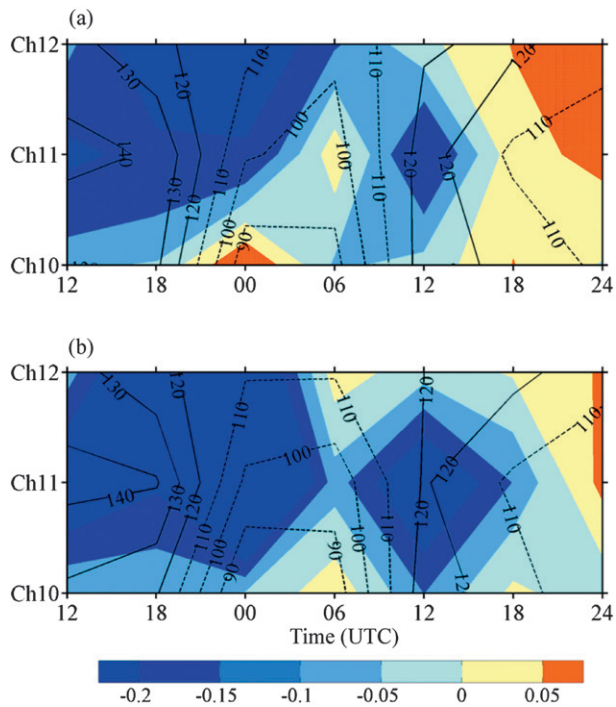

FIG. 10. Differences of the standard deviations (a) between experiments E7$_{GOES-Img}$ and CTRL$_{CONV}$ and (b) between experiments GE1$_{AMSU-A}$ and E1$_{AMSU-A}$ verified with GOES sounder observations from 1200 UTC 22 May to 2400 UTC 23 May 2008. Contours show data counts involved in the verification.

ratio and temperature between the other GOES imager single-channel experiments (E8$_{GOES-ch2}$, E9$_{GOES-ch3}$, or E11$_{GOES-ch5}$) and the control experiment CTRL$_{CONV}$ are rather small at 850 hPa. Larger analysis increments from assimilation of channel 4 in the low troposphere are associated with large $O - B$ differences for channel 4 than for other channels (figure omitted). It is encouraging to see a significant impact of window channel 4 on atmospheric moisture field in the low troposphere as it is not expected by its original design.

The adjustments in the upper levels introduced by imager radiance assimilation are more than an order of magnitude smaller than in the low troposphere. The GOES imager radiance assimilation reduces the water vapor and increases the temperature at 300 hPa (Fig. 7), with most of the differences between E7$_{GOES-Img}$ and CTRL$_{CONV}$ resulting from the assimilation of the *GOES-11/12* imager channel 3, an infrared channel that is mainly used for depicting the upper-level water vapor.

Results in Figs. 6 and 7 could be explained by examining the Jacobian of brightness temperature with respect to atmospheric temperature and moisture for channels 2–6 (Fig. 8). It is seen that the Jacobian of channel 4 with respect to temperature is rather narrow and reaches the maximum slightly below 850 hPa, while that for channel 5 is much broader. This implies that the mismatch between observed and model-simulated brightness temperatures are minimized through adjusting the temperature in the narrower layer of the atmosphere in the low troposphere for channel-4 data assimilation, and that for channel-5 data assimilation is achieved by adjusting a deeper layer of the atmosphere, resulting smaller analysis increments at a single level (e.g., 850 hPa; Fig. 6). The Jacobian of brightness temperature of channel 3 is largest in the upper-tropospheric layer, which is consistent with the results in Fig. 7.

b. *Adding GOES imager radiance to other satellite data*

Having compared a set of single satellite data assimilation impacts on QPFs over the Gulf of Mexico (section 3a), we conducted the second set of data assimilation experiments consisting of six dual types of satellite data assimilation experiments: GE1$_{AMSU-A}$, GE2$_{AIRS}$, GE3$_{HIRS/4}$, GE4$_{HIRS/3}$, GE5$_{MHS}$, and GE6$_{GSN}$, which are

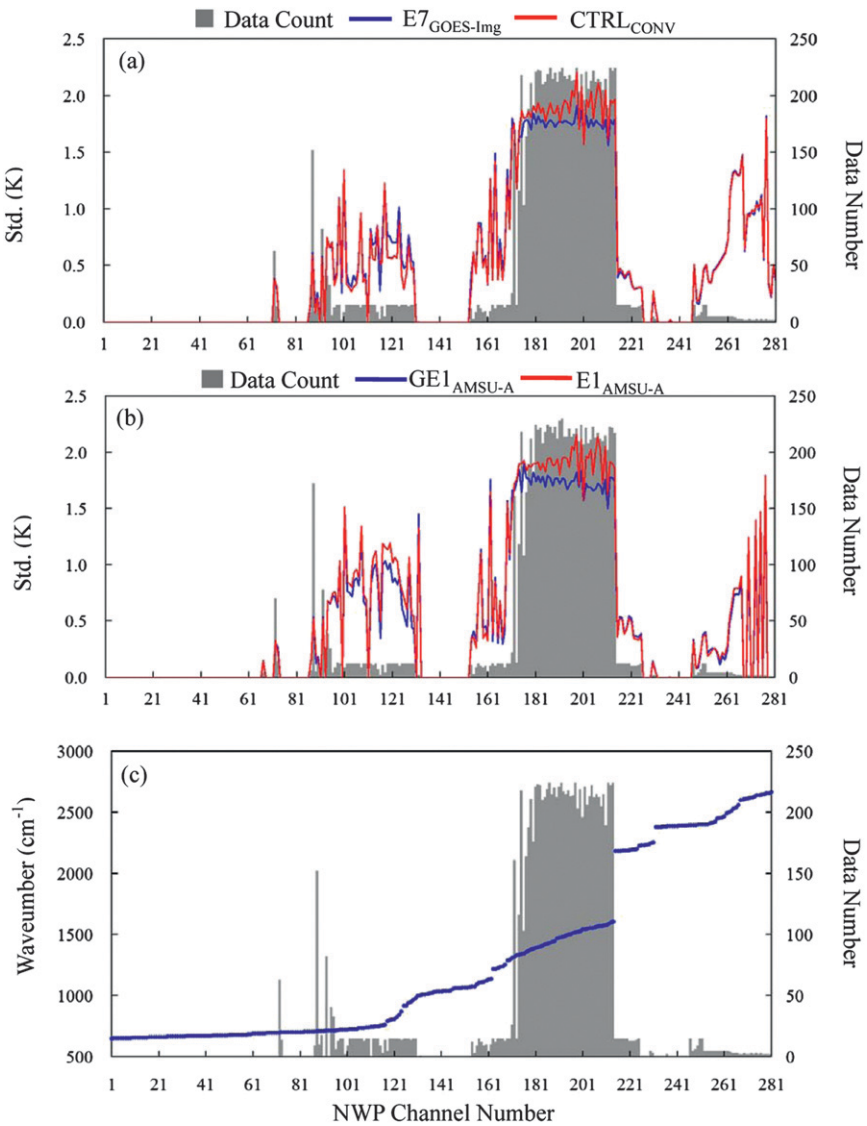

FIG. 11. Differences of the standard deviations (a) between experiments $E7_{GOES\text{-}Img}$ and $CTRL_{CONV}$ and (b) between experiments $GE1_{AMSU\text{-}A}$ and $E1_{AMSU\text{-}A}$ verified with AIRS observations at 1200 UTC 23 May 2008. Data counts involved in the verification are shown on the right axis (shaded). (c) The frequency of the 281 channels used in the verification.

similar to $E1_{AMSU\text{-}A}$, $E2_{AIRS}$, $E3_{HIRS/4}$, $E4_{HIRS/3}$, $E5_{MHS}$, and $E6_{GSN}$ except for adding GOES imager radiance measurements into the data assimilation procedure. These experiments are carried out to evaluate the added complementary benefits of GOES imager radiance measurements to other satellite data. The average 3-h threat score at 1-, 5-, 10-, and 15-mm thresholds from 0000 to 2400 UTC 23 May 2008 of forecasts without ($CTRL_{CONV}$, $E1_{AMSU\text{-}A}$, . . . , $E6_{GSN}$) and with ($E7_{GOES\text{-}Img}$, $GE1_{AMSU\text{-}A}$, . . . , $GE6_{GSN}$) GOES imager data are shown in Fig. 9. It is seen that GOES imager radiance data not only greatly complements conventional data, but also consistently brings positive impacts to all other satellite data assimilation. The experiments $E7_{GOES\text{-}Img}$, $GE1_{AMSU\text{-}A}$, $GE2_{AIRS}$, $GE3_{HIRS/4}$ outperform $CTRL_{CONV}$, $GE4_{HIRS/3}$, $GE5_{MHS}$, and $GE6_{GSN}$. Improvements for QPFs at 15-mm threshold are more than 50% when GOES imager radiances are added to conventional, AIRS, and HIRS/4 data, respectively.

To further examine the added values of GOES imager radiance assimilation, we compare the model forecasts with GSN radiance observations (see Fig. 10), which are available at all times (see Fig. 2). The standard deviations of the analyses and forecasts of experiments $E7_{GOES\text{-}Img}$

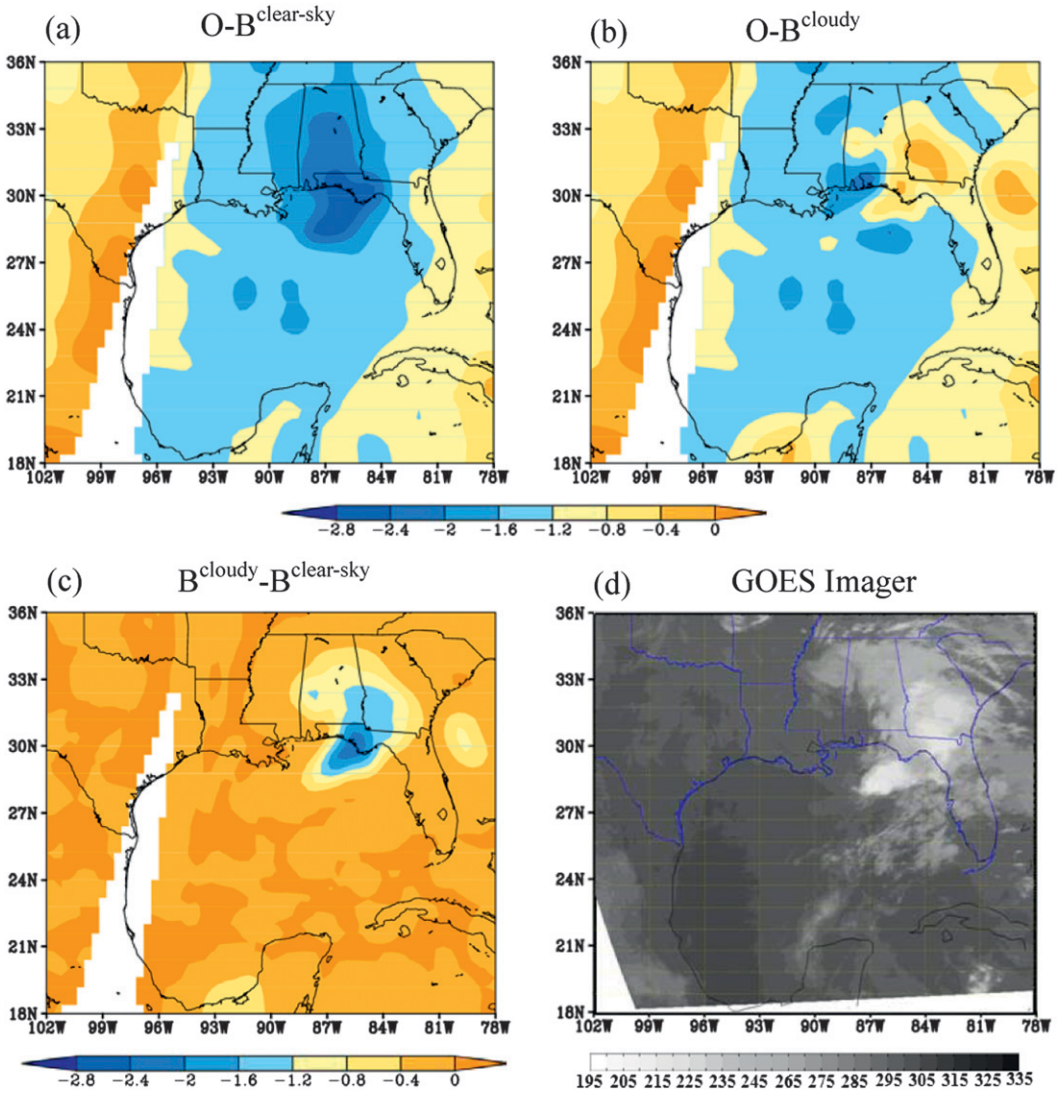

FIG. 12. Differences of brightness temperature of AMSU-A channel 6 between observations and the 12-h model forecast from the experiment $GE1_{AMSU\text{-}A}$ (a) without and (b) with considering cloud effect at 1200 UTC 23 May 2008. (c) Difference between (a) and (b) [i.e., (a) − (b)]. (d) Brightness temperatures from *GOES-11* imager channel 4.

are in general smaller than those of $CTRL_{CONV}$ and $E1_{AMSU\text{-}A}$ when verified with independent observations from GOES sounders. Improvements are found in both the entire 12-h data assimilation period (e.g., from 1200 UTC 22 May to 0000 UTC 23 May 2008) and the first 12-h forecast period (e.g., from 0000 UTC 23 May to 1200 UTC 23 May 2008).

The impacts of GOES imager radiance assimilation on model forecasts are also evaluated using AIRS observations, which are available in the model domain at 1200 UTC 23 May 2008 and can be used for validating the 12-h forecast. Please note that only those AIRS observations that pass GSI quality control are used for verification. Figure 11a compares the standard deviations of the 12-h forecasts from experiment $E7_{GOES\text{-}Img}$ with those of $CTRL_{CONV}$, and Fig. 11b compares the standard deviations of the 12-h forecasts from experiments $GE1_{AMSU\text{-}A}$ with those from $E1_{AMSU\text{-}A}$. For convenience, the frequency of the 281 channels involved in the verification as well as the data counts involved in the verification are also shown. The GOES imager radiance assimilation improves the model forecasts from both $CTRL_{CONV}$ and $E1_{AMSU\text{-}A}$ in the AIRS water vapor channels (channels 170–210). Forecast improvements are also seen when GOES imager radiance data is added to experiment $E1_{AMSU\text{-}A}$ in the AIRS CO_2

channels 90–130. A small degradation is noticed in the CO_2 channels for $E7_{GOES\text{-}Img}$ compared with $CTRL_{CONV}$.

Finally, we show in Figs. 12a,b the differences of brightness temperature between observations and the 12-h model forecast from experiment $GE1_{AMSU\text{-}A}$ at 1200 UTC 23 May 2008 without and with inputting the model-predicted cloud liquid water mixing ratio to CRTM. The brightness temperatures simulated with cloud effects considered is about 2° colder than without (see Fig. 12c) at the Gulf Coast. The location and shape of model-predicted cloud compares favorably with the observed cloud reflected in 4-km *GOES-11* imager channel 4 (Fig. 12d).

c. *All data experiments*

Having seen a consistent, positive impact of GOES imager radiance data to forecasts from a single type of satellite data experiments for all data types, the following question arises: "Does GOES radiance data assimilation bring any improvements to all data assimilation?" To answer this question, an experiment assimilating all types of satellite data in the GSI system, the experiment $AE1_{ALL}$ (without GOES imager data), is first carried out. It is surprising to discover that assimilation of all types of satellite data does not produce a better forecast than any single type of satellite data assimilation presented in section 3b. After comparing the results from many experiments with different combinations of various satellite data types, it is discovered that the inclusion of GSN and MHS data caused degradation of all-data experiments. The third set of data assimilation experiments are thus designed to demonstrate the degradation caused by the assimilation of GSN and MHS data and how GOES imager data affects the "all data" experiments with both GSN and MHS data eliminated. Figure 13 shows that threat scores of 3-h accumulative rainfall forecasts from three pairs of data assimilation experiments: ($AE1_{ALL}$, $GAE1_{ALL}$), ($AE2_{ALL\text{-}GSN}$, $GAE2_{ALL\text{-}GSN}$), and ($AE3_{ALL\text{-}MHS\text{-}GSN}$, $GAE3_{ALL\text{-}MHS\text{-}GSN}$) for the first two cases and ($AE1_{ALL}$, $GAE1_{ALL}$) and ($AE2_{ALL\text{-}GSN}$, $GAE2_{ALL\text{-}GSN}$) for the third case. The experiment pair ($AE3_{ALL\text{-}MHS\text{-}GSN}$, $GAE3_{ALL\text{-}MHS\text{-}GSN}$) is not conducted for the third case because of the lack of MHS data in the model domain for this case.

For three coastal QPFs near the Gulf of Mexico, elimination of GSN data from the GSI system ($AE2_{ALL\text{-}GSN}$) produces a better forecast than $AE1_{ALL}$. The forecast with both GSN and MHS data, $AE3_{ALL\text{-}MHS\text{-}GSN}$, is better than the forecasts from both $AE1_{ALL}$ and $AE2_{ALL\text{-}GSN}$. GOES imager radiance assimilation consistently improves the three all-data assimilation experiments for all three cases. The most significant

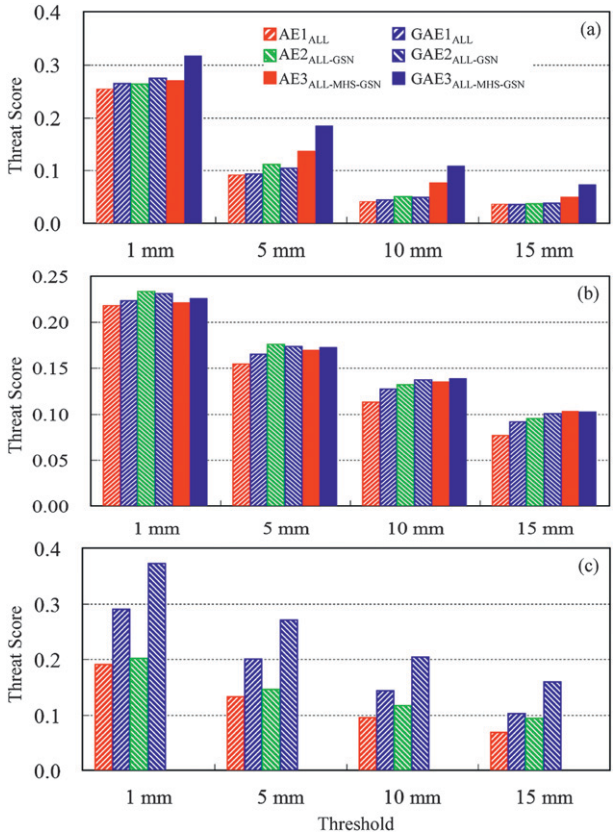

FIG. 13. Threat scores of 3-h accumulative rainfall averaged from 0000 to 2400 UTC 23 May 2008 from experiments $AE1_{ALL}$, $GAE1_{ALL}$, $AE2_{ALL\text{-}GSN}$, $GAE2_{ALL\text{-}GSN}$, $AE3_{ALL\text{-}MHS\text{-}GSN}$, and $GAE3_{ALL\text{-}MHS\text{-}GSN}$ at 1-, 5-, 10-, and 15-mm thresholds for case (a) 1, (b) 2, and (c) 3.

improvement the GOES imager radiance data assimilation made is achieved for case 1 when both GSN and MHS data types are eliminated and case 3 for the two scenarios tried (Fig. 13c).

Finally, causes for the degradation of including MHS data in the all-data experiment are analyzed. To show the sensitivity of MHS data assimilation to QC, two additional data assimilation experiments are carried out with a modified GOES imager assisted MHS QC algorithm, which only selects one MHS dataset that is closest to and within a 10-km distance from a GOES imager channel-3 clear-sky data point. The modified MHS QC algorithm thus keeps only clear-sky data points. These two new MHS sensitivity experiments will be denoted as $ME5_{MHS}$ and $MAE2_{ALL\text{-}GSN}$, which are the same as $E5_{MHS}$ and $AE2_{ALL\text{-}GSN}$ except for including only clear-sky MHS data collocated with GOES imager radiance data. Spatial distributions of data points of *NOAA-18* MHS brightness temperatures assimilated in $E5_{MHS}$ and $ME5_{MHS}$ at 1800 UTC 22 May 2008, are shown in

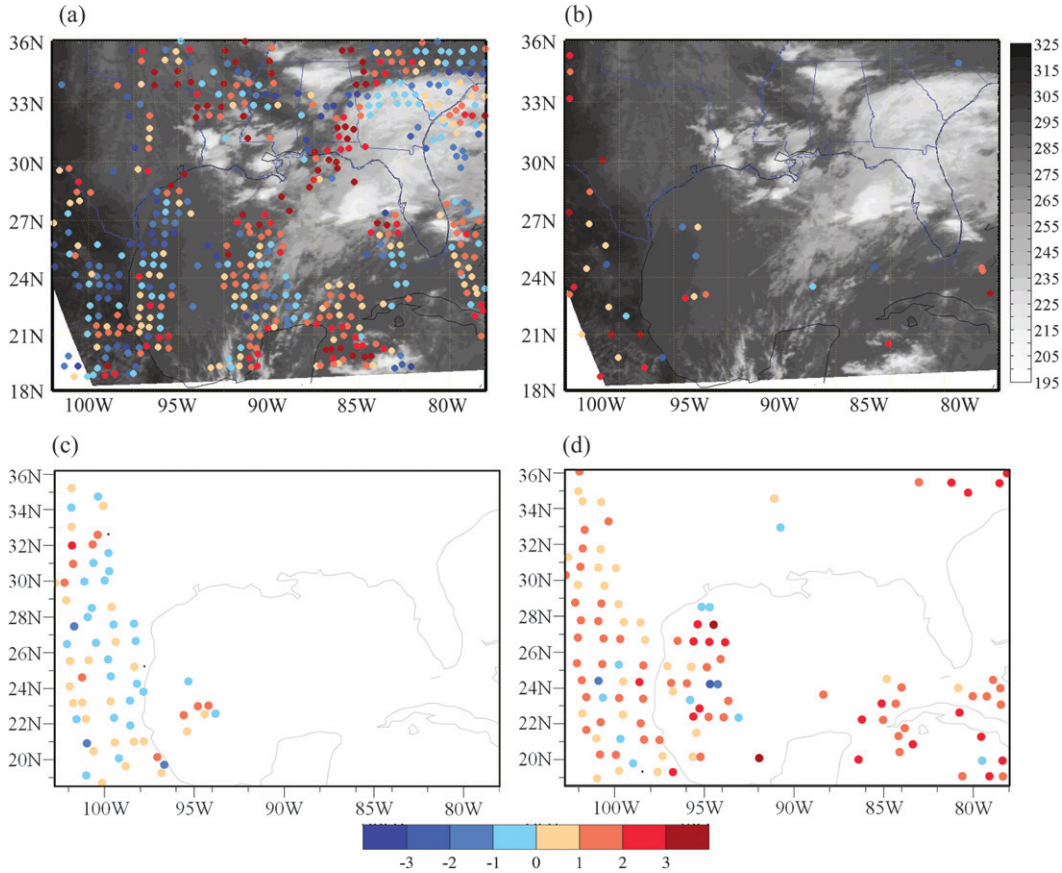

FIG. 14. Spatial distributions of data points of *NOAA-18* MHS brightness temperatures assimilated in (a) $E5_{MHS}$ and (b) $ME5_{MHS}$ at 1800 UTC 22 May 2008, with $O - B$ differences indicated in color. The 4-km *GOES-11* imager channel-4 brightness temperature field is shown in (a),(b) in black/white shading. Spatial distribution of data points of (c) *GOES-11* and (d) *GOES-12* imager channel 3 data that passes the quality control, with $O - B$ differences indicated in color as in (a),(b).

Figs. 14a,b, along with the 4-km *GOES-11* imager channel-4 brightness temperature field. The spatial distribution of data points of *GOES-11* and *GOES-12* imager channel-3 data that passes the quality control are shown in Figs. 14c,d. It is seen that MHS observations assimilated in $ME5_{MHS}$ and $MAE2_{ALL\text{-}GSN}$ are significantly reduced and are located in clear-sky regions.

Figure 15a presents threat scores of 3-h accumulative rainfall forecasts from experiments $E5_{MHS}$, $ME5_{MHS}$, $AE2_{ALL\text{-}GSN}$, and $MAE2_{ALL\text{-}GSN}$ at 1-, 5-, 10-, and 15-mm thresholds averaged from 0000 to 2400 UTC 23 May 2008. The threat scores of 3-h accumulative rainfall at 5- and 10-mm thresholds on 23 May 2008 are shown in Figs. 15b,c. The assimilation of only clear-sky MHS data produced better QPFs than the assimilation of cloud-contaminated MHS observations, especially after 6 h into the model forecasts. The fact that an elimination of MHS data over areas where GOES detects clouds significantly improved the MHS data assimilation results suggests an urgent need for an improved MHS radiance assimilation including improved quality control, bias correction, and microphysics parameterization.

4. Summary and conclusions

This is a case study assessing the added values of *GOES-11/12* imager radiance data to other satellite data for improved coastal precipitation forecasts using the NCEP GSI analysis system and the regional ARW forecast model. The GOES imager radiance is simulated by CRTM incorporated in GSI. First, the added values of GOES imager radiance to conventional data for improved coastal QPFs near the northern Gulf of Mexico was compared with those from other six satellite instruments. It is found that GOES

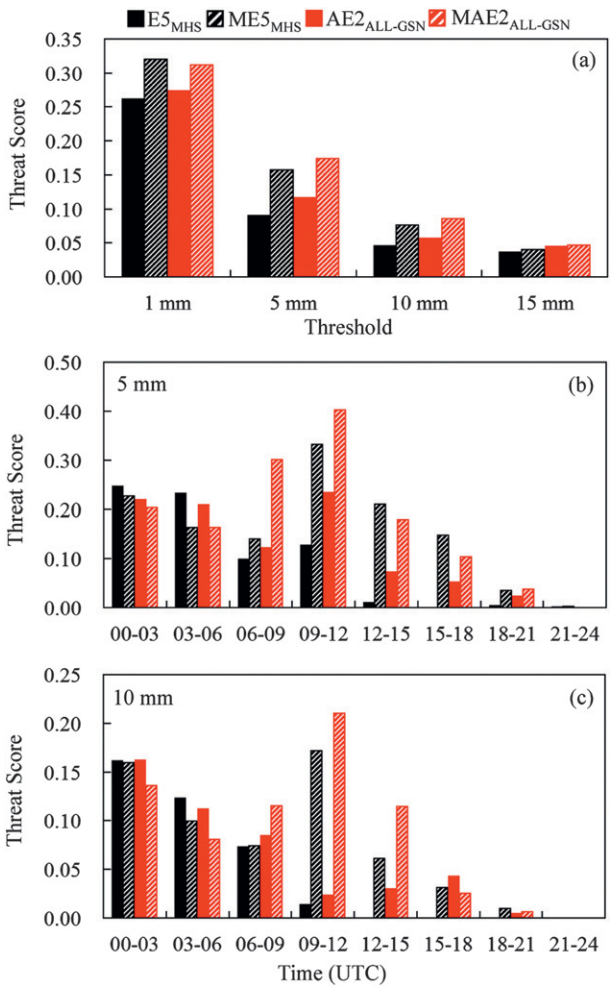

FIG. 15. (a) Threat scores of 3-h accumulative rainfall forecasts from experiments $E5_{MHS}$, $ME5_{MHS}$, $AE2_{ALL\text{-}GSN}$, and $MAE2_{ALL\text{-}GSN}$ at 1-, 5-, 10-, and 15-mm thresholds averaged from 0000 to 2400 UTC 23 May 2008. Threat scores of 3-h accumulative rainfall at (b) 5- and (c) 10-mm thresholds during 0000 to 2400 UTC 23 May 2008.

imager data produces the largest added value to conventional data for improved QPFs. Out of six different GOES imager channels, the surface-sensitive infrared channel 4 (10.7 μm) on board both *GOES-11/12* contributes most significantly to the improvement, and the CO_2 surface-sensitive infrared channel 6 (13.3 μm) on board *GOES-12* is of secondary importance. Second, the values of GOES imager radiance added to six different types of satellite instruments are assessed. It is shown that assimilation of GOES imager radiances during a 12-h time window prior to convective initiation and/or development contributes positively to any single type of satellite data for improved QPFs near the Gulf Coast. However, it is realized that none of the forecasts is particularly good. An in-depth investigation on quality control, channel selection, and bias correction for each type of satellite data in the GSI system is required for any further improvements of QPFs.

Third, it is pointed out that assimilation of all types of satellite data in the GSI system did not produce a better forecast than any single type of satellite data assimilation, especially when the 3-h accumulative rainfall exceeds 10 mm. The problems with the all-satellite-data assimilation are found to arise from the inclusions of MHS and GSN data. Finally, we show that an elimination of MHS data over areas where GOES detects clouds improved the MHS data assimilation results, suggesting that an improved quality control algorithm is urgently required for MHS data assimilation.

This is our second study on GOES imager radiance assimilation following the work by Zou et al. (2011). Before exploring the full potential of GOES high temporal (3–15 min) and spatial resolutions (4–8 km) data as originally planned, the problems with an ineffective assimilation of MHS and GSN data in GSI will be thoroughly analyzed.

This study only investigated impacts of direct assimilation of GOES imager radiance for a real case event. Results about positive impacts of GOES imager radiance assimilation experiments and forecast degradations by MHS and GSN data assimilation could be case dependent. We plan to repeat these experiments over a longer period of time and for different weather systems to see if the conclusions from this case study could be generalized.

Acknowledgments. This work was jointly supported by the Chinese Ministry of Science and Technology under 973 Project (2010CB951600), NOAA GOES-R Risk Reduction Program, and a project funded by the Priority Academic Program Development of Jiangsu Higher Education Institutions (PAPD). The views and opinions contained in this paper reflects those of the authors and should not be construed as an official National Oceanic and Atmospheric Administration or U.S. government position, policy, or decision.

REFERENCES

Anderson, D., and Coauthors, 2007: Development of the ECMWF seasonal forecast System 3. ECMWF Tech. Memo. 503, 56 pp. [Available online at www.ecmwf.int.]

Andersson, E., J. Pailleux, J.-N. Thépaut, J. R. Eyre, A. P. McNally, G. A. Kelly, and P. Courtier, 1994: Use of cloud-cleared radiances in three/four-dimensional variational data assimilation. *Quart. J. Roy. Meteor. Soc.,* **120,** 627–653.

Anthes, R. A., Y. Kuo, E. Hsie, S. Low-Nam, and T. W. Bettge, 1989: Estimation of skill and uncertainty in regional numerical models. *Quart. J. Roy. Meteor. Soc.,* **115,** 763–806.

Aumann, H. H., and Coauthors, 2003: AIRS/AMSU/HSB on the Aqua mission: Design, science objectives, data products, and processing systems. *IEEE Trans. Geosci. Remote Sens.,* **41,** 253–264.

Derber, J. C., and W.-S. Wu, 1998: The use of TOVS cloud-cleared radiances in the NCEP SSI analysis system. *Mon. Wea. Rev.,* **126,** 2287–2299.

Eyre, J. R., G. Kelly, A. P. McNally, E. Andersson, and A. Persson, 1993: Assimilation of TOVS radiance information through onedimensional variational analysis. *Quart. J. Roy. Meteor. Soc.,* **119,** 1427–1463.

Garand, L., and J. Hallé, 1997: Assimilation of clear- and cloudy-sky upper-tropospheric humidity estimates using *GOES-8* and *GOES-9* data. *J. Atmos. Oceanic Technol.,* **14,** 1036–1054.

Goerss, J. S., C. S. Velden, and J. D. Hawkins, 1998: The impact of multispectral *GOES-8* wind information on Atlantic tropical cyclone forecasts in 1995. Part II: NOGAPS forecasts. *Mon. Wea. Rev.,* **126,** 1219–1227.

Han, Y., F. Weng, Q. Liu, and P. van Delst, 2007: A fast radiative transfer model for SSMIS upper atmosphere sounding channels. *J. Geophys. Res.,* **112,** D11121, doi:10.1029/2006JD008208.

Köpken, C., G. Kelly, and J.-N. Thépaut, 2004: Assimilation of Meteosat radiance data within the 4D-Var system at ECMWF: Assimilation experiments and forecast impact. *Quart. J. Roy. Meteor. Soc.,* **130,** 2277–2292.

McMillin, L., and H. Fleming, 1976: Atmospheric transmittance model of an absorbing gas: A computationally fast and accurate model for absorbing gases with constant mixing ratios in inhomogeneous atmospheres. *Appl. Opt.,* **15,** 358–363.

McNally, A. P., P. D. Watts, J. A. Smith, R. Engelen, G. A. Kelly, J. N. Thépaut, and M. Matricardi, 2006: The assimilation of AIRS radiance data at ECMWF. *Quart. J. Roy. Meteor. Soc.,* **132,** 935–957.

Menzel, W. P., and J. F. W. Purdom, 1994: Introducing GOES-I: The first of a new generation of geostationary operation environmental satellites. *Bull. Amer. Meteor. Soc.,* **75,** 757–781.

Mo, T., 1996: Prelaunch calibration of the Advanced Microwave Sounding Unit-A for NOAA-K. *IEEE Trans. Microwave Theory Technol.,* **44,** 1460–1469, doi:10.1109/22.536029.

——, 1999: AMSU-A antenna pattern corrections. *IEEE Trans. Geosci. Remote Sens.,* **37,** 103–112.

Nieman, S. J., J. Schmetz, and W. P. Menzel, 1993: A comparison of several techniques to assign heights to cloud tracers. *J. Appl. Meteor.,* **32,** 1559–1568.

Purser, R. J., W.-S. Wu, D. F. Parrish, and N. M. Roberts, 2003a: Numerical aspects of the application of recursive filters to variational statistical analysis. Part I: Spatially homogeneous and isotropic Gaussian covariances. *Mon. Wea. Rev.,* **131,** 1524–1535.

——, ——, ——, and ——, 2003b: Numerical aspects of the application of recursive filters to variational statistical analysis. Part II: Spatially inhomogeneous and anisotropic general covariances. *Mon. Wea. Rev.,* **131,** 1536–1548.

Rao, P. A., C. S. Velden, and S. A. Braun, 2002: The vertical error characteristics of GOES-derived winds: Description and experiments with numerical weather prediction. *J. Appl. Meteor.,* **41,** 253–271.

Saunders, R. W., M. Matricardi, and P. Brunel, 1999: An improved fast radiative transfer model for assimilation of satellite radiance observations. *Quart. J. Roy. Meteor. Soc.,* **125,** 1407–1425.

Saunders, R., and Coauthors, 2007: A comparison of radiative transfer models for simulating Atmospheric Infrared Sounder (AIRS) radiances. *J. Geophys. Res.,* **112,** D01S90, doi:10.1029/2006JD007088.

Soden, B. J., C. S. Velden, and R. E. Tuleya, 2001: The impact of satellite winds on experimental GFDL hurricane model forecasts. *Mon. Wea. Rev.,* **129,** 835–852.

Stengel, M., P. Undén, M. Lindskog, P. Dahlgren, N. Gustafsson, and R. Bennartz, 2009: Assimilation of SEVIRI infrared radiances with HIRLAM 4D-Var. *Quart. J. Roy. Meteor. Soc.,* **135,** 2100–2109.

Szyndel, M. D. E., J.-N. Thépaut, and G. Kelly, 2005: Evaluation of potential benefit of SEVIRI water vapour radiance data from *Meteosat-8* into global numerical weather prediction analyses. *Atmos. Sci. Lett.,* **6,** 105–111.

Tomassini, M., G. Kelly, and R. Saunders, 1999: Use and impact of satellite atmospheric motion winds on ECMWF analyses and forecasts. *Mon. Wea. Rev.,* **127,** 971–986.

Velden, C. S., 1996: Winds derived from geostationary satellite moisture channel observations: Applications and impact on numerical weather prediction. *Meteor. Atmos. Phys.,* **60,** 37–46.

——, C. M. Hayden, S. J. Nieman, W. P. Menzel, S. Wazong, and J. S. Goerss, 1997: Upper tropospheric winds derived from geostationary satellite water vapor observations. *Bull. Amer. Meteor. Soc.,* **78,** 173–195.

——, T. L. Olander, and S. Wazong, 1998: The impact of multispectral *GOES-8* wind information on Atlantic tropical cyclone track forecasts in 1995. Part I: Dataset methodology, description, and case analysis. *Mon. Wea. Rev.,* **126,** 1202–1218.

Weng, F., 2007: Advances in radiative transfer modeling in support of satellite data assimilation. *J. Atmos. Sci.,* **64,** 3799–3807.

Wu, W.-S., R. J. Purser, and D. F. Parrish, 2002: Three-dimensional variational analysis with spatially inhomogeneous covariances. *Mon. Wea. Rev.,* **130,** 2905–2916.

Zou, X., Q. Xiao, A. E. Lipton, and G. D. Modica, 2001: A numerical study of the effect of GOES sounder cloud-cleared brightness temperatures on the prediction of Hurricane Felix. *J. Appl. Meteor.,* **40,** 34–55.

——, Z. Qin, and F. Weng, 2011: Improved coastal precipitation forecasts with direct assimilation of *GOES-11/12* imager radiances. *Mon. Wea. Rev.,* **139,** 3711–3729.